AUT Journal of Electrical Engineering

AUT J. Elec. Eng., 58(1) (2026) 59-74
DOI: 10.22060/eej.2025.24329.5685

Hilbert-Mel Frequency Spectrum Features for Efficient EEG-Based Alzheimer's Detection

Maryam Bahmani[1], Hossein Marvi[1]*, Hossein Khosravi[1], Vahid Abolghasemi[2]

[1] Faculty of Electrical Engineering, Shahrood University of Technology, Iran.
[2] School of Computer Science and Electronic Engineering, University of Essex, Colchester, UK.

ABSTRACT: Alzheimer's disease (AD) is a progressive neurodegenerative disorder that severely impairs cognitive function and disrupts brain connectivity. Early and accurate diagnosis is crucial for effective intervention, yet identifying discriminative features from complex electroencephalography (EEG) signals remains a challenge. Resting-state EEG provides a non-invasive and cost-effective tool for AD detection, but its diagnostic utility is highly dependent on the quality of extracted features. This study introduces a novel feature extraction approach that uses Mel-Frequency Spectrum Features (MFS) and the Hilbert Transform (HT) to enhance both spectral and temporal feature representation of EEG signals. The proposed Hilbert-Mel Frequency Spectrum (HMFS) framework captures subtle variations in phase and amplitude, providing a rich and complementary set of descriptors. Principal Component Analysis (PCA) is employed to reduce dimensionality while retaining key information, enabling more efficient and accurate classification. A 5-fold cross-validation approach was employed to assess model performance and generalizability. The extracted features are classified using various machine learning models, with K-Nearest Neighbors (KNN) achieving the highest performance. The proposed method reached an accuracy of 99.24% with a perfect recall of 100%, precision of 98.61%, specificity of 98.39%, F1-score of 99.30%, and geometric mean score of 99.31%. Compared to existing EEG-based AD detection techniques, the HMFS method surpasses previous approaches in accuracy and recall, and it achieves higher performance. The integration of spectral and temporal features results in a more robust feature space, thereby improving generalization. This approach provides a reliable, efficient framework for early AD diagnosis with potential clinical applications.

Review History:

Received: Jun. 29, 2025
Revised: Oct. 22, 2025
Accepted: Nov. 14, 2025
Available Online: Jan. 10, 2026

Keywords:

EEG Signals
Alzheimer's Disease (AD)
Mel-Frequency Spectrum (MFS)
Hilbert Transform (HT)
Principal Component Analysis (PCA)

1- Introduction

Dementia is a collective term encompassing various conditions that negatively affect memory, cognitive function, and daily life [1]. Among the different types of dementia, Alzheimer's disease (AD) is the most prevalent form. With the global prevalence of AD steadily increasing, early detection plays a crucial role in preventing memory loss and cognitive decline. The World Health Organization (WHO) estimates that more than 55 million people worldwide suffer from dementia [2]. In 2020, approximately 50 million people were affected by AD, and projections indicate that this figure will double every five years, reaching 75 million by 2030 and 152 million by 2050 [3, 4]. Electroencephalography (EEG), a non-invasive and cost-effective neuroimaging technique, has emerged as a promising tool for early AD diagnosis [5]. EEG captures brain activity with high temporal resolution, enabling the detection of subtle neural abnormalities associated with AD. Over the past decade, researchers have developed a range of computational methods to analyze EEG signals for AD detection. These include traditional signal processing techniques such as wavelet coherence, fractal dimension, and visibility graphs [6], alongside more recent advances in deep learning and signal decomposition [7].

A variety of computational approaches have been employed to extract relevant features and improve classification accuracy. For example, deep learning models have been developed to capture patterns in short EEG segments by analyzing spectral, complexity, and synchrony characteristics. Song et al. in [8], use a three-path deep encoder combined with a transfer learning-based model and a modified generative adversarial module. Additionally, signal decomposition methods such as empirical mode decomposition (EMD) and discrete wavelet transform (DWT) have demonstrated high accuracy in differentiating between EEG recordings from AD patients and healthy individuals [9].

In [5] A low-complexity wavelet filter bank (LCOWFBs-v) was evaluated using fractal dimension features, specifically Higuchi's fractal dimension (HFD) and Katz's fractal dimension (KFD). The importance of these

*Corresponding author's email: h.marvi@shahroodut.ac.ir

features was assessed with the Kruskal-Wallis test, and a cubic support vector machine (SVM) classifier achieved an accuracy of 98.5% via 10-fold cross-validation. Similarly, in [10], decomposition techniques including brain frequency band filtering, DWT, and EMD were paired with classifiers such as SVM, K-nearest neighbors (KNN), and regularized linear discriminant analysis (RLDA). To address the challenges posed by limited and imbalanced EEG datasets, data augmentation methods such as variational autoencoders (VAEs) and noise injection have also been employed [11].

Puri et al. in [12] applied EMD to generate nine intrinsic mode functions (IMFs) from EEG signals, extracting ten statistical and nonlinear features from them. Key features were selected using the Kruskal-Wallis test, focusing on Hjorth parameters—activity, mobility, and complexity. Other signal processing methods, such as wavelet coherence, quadratic entropy, quantile graphs, and visibility graphs, have also proven effective in differentiating AD patients from healthy controls [13]. In [14], Biomarkers extracted from resting-state EEG achieved over 70% accuracy in classifying healthy controls, mild cognitive impairment (MCI) patients, and AD patients. The study concluded that combining EEG data with cerebrospinal fluid (CSF) biomarkers and demographic information yielded the best results. AlSharabi et al. in [15] used an elliptical digital bandpass filter to clean EEG signals and applied DWT to extract features from different frequency bands. Features such as logarithmic band power, standard deviation, and kurtosis were used to enhance diagnostic accuracy.

Xia et al. in [16] introduced a classification framework using resting-state EEG from AD, MCI, and healthy control groups. To mitigate data scarcity and overfitting, they applied overlapping sliding windows for augmentation and trained a modified deep pyramid convolutional neural network (DPCNN), achieving 97.10% average accuracy with 5-fold cross-validation. Houmani et al. in [17] created an automated EEG diagnostic system for clinical settings, using data from 169 patients with various cognitive impairments, including subjective cognitive impairment (SCI), MCI, possible AD, and other conditions. They found that two features, epoch-based entropy and bump modeling, effectively distinguished between these groups.

Chen et al. in [18] introduced a hybrid model combining CNNs and vision transformers (ViTs) to enhance feature extraction in EEG data. Their Dual-Branch feature fusion network (DBN) integrates CNN and ViT components to capture texture and global semantics. Spatial attention (SA) and channel attention (CA) were incorporated to improve the detection of abnormal EEG patterns, supported by a two-factor decision strategy for enhanced prediction accuracy. Recurrent neural networks (RNNs) [19] and LSTMs [20] are also commonly used in EEG analysis due to their ability to model temporal dependencies and handle variable-length inputs. However, their high computational complexity and long training times make them less practical for large-scale EEG datasets. The choice of classification architecture is therefore often influenced by trade-offs between accuracy, scalability, and training efficiency. Table 1 summarizes key EEG-based approaches for AD diagnosis.

Although EEG-based diagnosis of AD has attracted increasing research attention, several critical methodological and interpretive challenges remain unaddressed. A majority of prior studies treat spectral and temporal features in isolation, overlooking their potential synergy in capturing robust biomarkers of AD. This fragmented treatment undermines both the interpretability of EEG-derived features and their diagnostic reliability. Moreover, few studies conduct systematic comparisons of different signal processing pipelines, making it difficult to determine optimal configurations. Although multiband and hybrid feature extraction methods hold promise for integrating fine-grained frequency information with transient temporal dynamics, such approaches remain underexplored and underdeveloped. Additionally, the use of ensemble learning and advanced time-frequency representations is still limited, while commonly used techniques like wavelet transforms suffer from redundancy and sensitivity to parameter tuning. These gaps highlight the need for comprehensive frameworks that integrate spectral and temporal representations in a scalable, interpretable, and diagnostically robust manner.

To address these limitations, we propose a novel dual-domain framework that integrates both spectral and temporal features of EEG signals in a unified and computationally efficient manner. Our approach combines the MFS, which captures perceptually relevant spectral information, with HT, which extracts envelope and phase dynamics from the time domain. This combination enables a more holistic representation of EEG activity, overcoming the limitations of conventional single-domain analyses. To enhance efficiency and reduce redundancy, PCA is applied for dimensionality reduction, preserving key discriminative features while ensuring scalability. The effectiveness of the proposed features is validated through a comparative analysis of various classifiers, with the KNN algorithm achieving superior performance in distinguishing AD patients from healthy individuals. Moreover, by applying a 5-fold cross-validation strategy on a publicly available and sufficiently large dataset, the study ensures rigorous performance evaluation and avoids common pitfalls such as data leakage and overfitting.

The remainder of the paper is structured as follows. Section 2 presents the proposed dual-domain feature extraction framework in detail, along with the dataset and preprocessing steps. Section 3 reports the experimental results and performance comparison across classifiers. Section 4 discusses the implications of the findings in the context of existing literature. Section 5 concludes the paper with a summary and directions for future research.

2- Methodology

The proposed framework for AD detection presents a novel methodology that uses Mel Cepstrum and the HT to achieve robust and comprehensive feature extraction from EEG signals. This approach addresses key limitations

Table 1. Summary of recent EEG-based AD detection studies, including methods, features, and datasets.

Authors	Method	Dataset
Puri et al., 2023 [5]	low-complexity orthogonal wavelet filter banks Higuchi's fractal dimension, Katz's fractal dimension, SVM	23 subjects (AD-12, NC-11)
Vicchietti et al., 2023 [13]	Wavelet coherence, Fractal dimension, Quadratic entropy, Wavelet energy, Quantile graphs, Visibility graphs	184 subjects (AD-160, NC-24)
AlSharabi et al., 2022 [15]	band-pass elliptic digital filter, DWT, logarithmic band power, standard deviation, variance, kurtosis, average energy, root mean square, Norm	88 subjects (AD-31, MCI-22, NC-35)
Chen et al., 2023 [18]	Dual-Branch Feature Fusion Network (DBN) using CNN and ViTs	88 subjects (AD-36, FTD-23, NC-29)
Sekhar et al., 2023 [21]	GAN, MPA, LSTM	13 subjects (AD-7, NC-6)
Cao et al., 2024 [22]	EBC, PSD, DSL-GNN	60 subjects (AD-20, HC-20, PD-20)
Al-Nuaimi et al., 2018 [23]	LZC, TsEn, HFD	11 subjects (AD-3, NC-8)
Pirrone et al., 2022 [24]	CWT-based average magnitude of SBs, LDA	105 subjects (AD-48, MCI-37, NC-20)
Kulkarni et al., 2017 [25]	DWT with db3-based features	100 subjects (AD-50, NC-50)
Durongbhan et al., 2019 [26]	CWT-based average magnitude of SBs	28 subjects (AD-8, NC-20)

of conventional methods, which often prioritize either spectral or temporal characteristics in isolation, leading to incomplete signal representations. By combining the spectral decomposition capabilities of the Mel Cepstrum with the phase and instantaneous energy analysis enabled by HT, the proposed framework captures both complementary and nuanced signal features critical for accurate AD detection. The model employs sequential layers designed to extract and integrate multiscale patterns across spectral and temporal domains, providing a comprehensive representation of EEG signals. Such hierarchical feature synthesis enables the identification of subtle signal variations and higher-order abstractions that are challenging to discern using traditional approaches.

The methodological pipeline, as illustrated in Fig. 1, consists of five critical stages: (1) data acquisition, (2) pre-processing, (3) feature extraction, (4) dimensionality reduction, and (5) classification. Each stage plays a critical role in ensuring accurate and scalable EEG-based AD detection. The overall framework is designed to integrate spectral and temporal information in a unified manner, enhance signal quality, reduce feature space complexity, and optimize classification accuracy. Detailed descriptions of each component are provided in the subsequent sections.

To evaluate the effectiveness of the extracted features, multiple classifiers were employed, including KNN, SVM, Decision Trees (DT), AdaBoost, GradientBoost, and Random Forest (RF). These classifiers, widely recognized in the field of biomedical signal processing for their effectiveness and computational efficiency, were rigorously optimized through experimental evaluation to ensure robust performance. Further technical details, including parameter configurations and implementation specifics, are provided in [27-29].

2- 1- Dataset and pre-processing

The EEG dataset used in this study, known as the AZD dataset, is publicly available and was collected by the University Hospital of Valladolid in Spain. The dataset includes 23 individuals: 12 with AD and 11 with HC were enrolled [30-32]. Subjects belonging to both classes were recruited from the Alzheimer's Patients' Relatives Association of Valladolid. Rigorous screening was conducted to ensure that HC participants had no current or prior neurological conditions. The 16-channel (Fp1, Fp2, P3, P4, C3, C4, O1, O2, T3, T4, T5, T6, F3, F4, F7, and F8) EEG recorder built in accordance with the international

Table 2. Demographic characteristics of subjects in the AZD EEG dataset.

Class	AD	HC
Total subjects	12	11
Males	5	7
Females	7	4
Age (mean±SD)	72.8 ± 6.1 years	72.8 ± 6.1 years

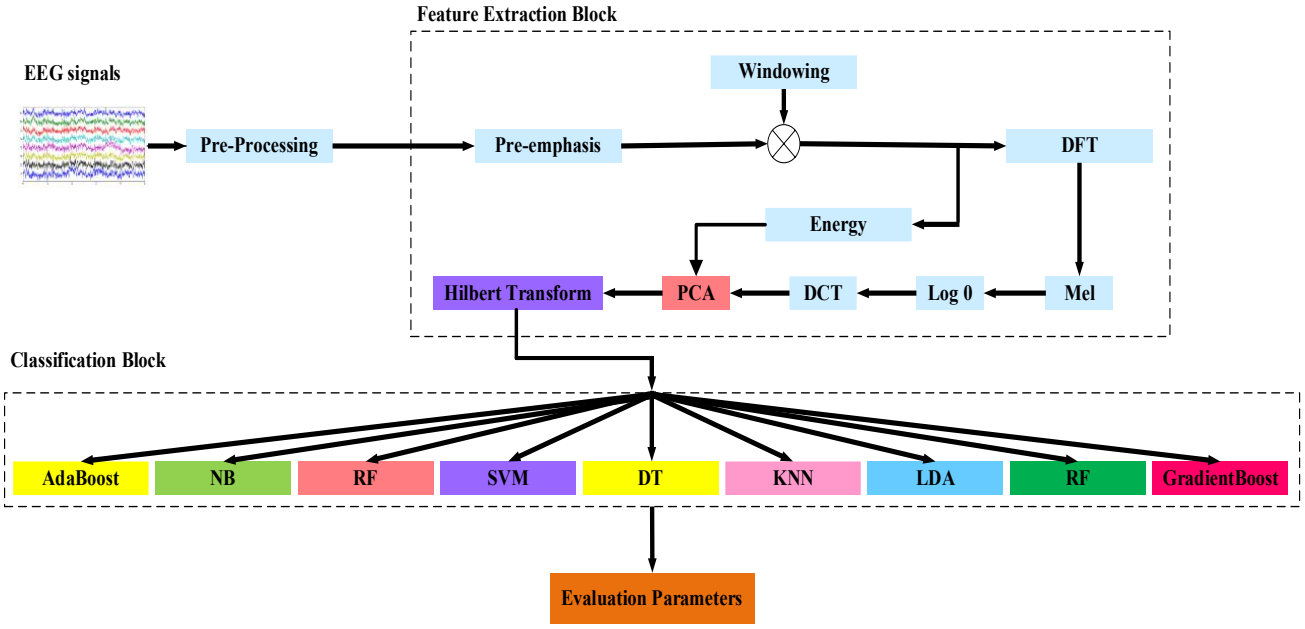

Fig. 2. Block diagram of the proposed HMFS feature extraction method.

10–20 system has been used for the signal acquisition. EEG signals were captured with participants' eyes closed during a resting state to minimize disturbances. These AD patients underwent a detailed clinical evaluation, including brain scans and cognitive assessments using the Mini-Mental State Examination (MMSE) [33]. The average MMSE score for the AD group was 13.2 ± 5.92 points, indicating varying levels of cognitive decline.

In the preprocessing phase, in order to eliminate power line interference and various artifacts, a band-pass filter with cutoff frequencies at 0.5 and 60 Hz is applied to each signal. Each EEG epoch lasted 5 seconds (1280 data points) and was sampled at 256 Hz using a 12-bit analog-to-digital converter. Following preprocessing, a total of 9849 clean and artifact-free EEG epochs were identified, with 5648 from Alzheimer's disease patients and 4201 from NC subjects [34]. The distribution of AD and HC subjects within the groups is outlined in Table 2.

2- 2- Proposed Hilbert-Mel feature extraction method

This section introduces a novel feature extraction methodology designed to capture the subtle spectral and temporal dynamics of EEG signals for the purpose of AD detection. The proposed approach builds upon and significantly enhances conventional cepstral analysis by integrating Mel-scaled spectral information with phase-sensitive temporal cues extracted via the Hilbert Transform. This dual-domain strategy enables a richer, more discriminative representation of neural activity patterns, which are often missed when using time- or frequency-based features in isolation.

The complete processing pipeline—from pre-emphasis to the construction of analytic signals—is illustrated in Fig. 2. Each stage has been carefully designed to retain clinically relevant EEG characteristics while minimizing information loss and redundancy. The subsequent subsections provide a step-by-step technical breakdown of the method.

The proposed feature extraction method begins with pre-

emphasis following the pre-processing stage. Pre-emphasis is designed to counteract the attenuation of high-frequency components in the input signal. By applying this technique, the suppressed high-frequency elements are restored to their original levels. For a given signal $x[n]$, the pre-emphasized signal $y[n]$ is mathematically expressed as Eq. (1):

$$y[n] = x[n] - \alpha x[n-1] \tag{1}$$

where α typically ranges from 0.93 to 0.97, with a common value of 0.97 utilized in this study. This pre-emphasis step effectively restores the high-frequency components, ensuring that these are better represented for subsequent analysis. Next, the pre-emphasized signal is divided into frames of length N through a process known as framing, ensuring that each frame is stationary. Each frame typically lasts between 20 and 40 milliseconds. If $y[n]$ is the pre-emphasized signal, the m_{th} sample in the i_{th} frame $s_i[m]$ is defined as Eq. (2):

$$S_i[m] = y[iR + m] \tag{2}$$

where R denotes the frame shift size, typically optimized based on signal characteristics. Windowing is applied to each frame using a Hamming window to reduce edge effects as Eq. (3):

$$w(n) = \begin{cases} 0.54 - 0.46\cos(2\pi \frac{n}{N-1}), & 0 \le n \prec N \\ 0, & o w \end{cases} \tag{3}$$

Thus, the windowed frame $x_i[m]$ is expressed as Eq. (4):

$$x_i[m] = S_i[m]\, w[m] \tag{4}$$

Following the windowing process, the Discrete Fourier Transform (DFT) $X_i[k]$ of each windowed frame $x_i[m]$ is calculated as Eq. (5):

$$X_i[k] = \sum_{n=0}^{N-1} x_i[n] e^{-\frac{j2\pi kn}{N}}, \quad 0 \le n,\ k \le N-1 \tag{5}$$

where j represents the imaginary unit. The power spectrum $P_i[k]$ of each frame is subsequently computed as Eq. (6):

$$P_i[k] = |X_i[k]|^2 \tag{6}$$

After obtaining the DFT, the next step is to process these coefficients through triangular Mel filter banks. The Mel scale is used to transform the frequencies into a more perceptually meaningful scale. The conversion from frequencies in Hertz to the Mel scale is performed using Eq. (7):

$$f_{mel} = 2595\ \log_{10}(1 + \frac{f}{700}) \tag{7}$$

The filter bank energies $E_i[m]$ are computed by processing the power spectrum $P_i[k]$ through the triangular Mel filter banks, which can be seen in Fig. 3, as expressed by Eq. (8):

$$E_i[m] = \sum_{k=0}^{N-1} P_i[k]\, H_m[k], \quad o \le m \le M \tag{8}$$

Where $H_m[k]$ represents the m_{th} Mel filter, and M is the number of filters used in the band. To capture uncorrelated features, the Discrete Cosine Transform (DCT) is applied to the output of the Mel filter banks as Eq. (9):

$$c_i[n] = \sqrt{\frac{2}{M}} \sum_{m=0}^{M-1} \log(E_i[m]) \cos(\frac{n\pi(m-0.5)}{M}), \quad n = 1,\ 2,\ ...,L \tag{9}$$

where L denotes the number of output coefficients, and $c_i[n]$ are the cepstral coefficients. These coefficients represent a reduced-dimensional representation of the original features, minimizing redundancy. At this point, the feature dimensions are initially $(N, M \times L)$, which are large and need to be reduced for efficient computation. To achieve this, PCA is applied to the cepstral coefficients. PCA helps reduce the dimensionality by selecting the most discriminative components while maintaining the integrity of the signal's features. The feature space is reduced to (N, l), where l is significantly smaller than $M \times L$. Finally, the HT is applied to the output of the PCA stage to extract instantaneous amplitude and characteristics. The Hilbert transform H is mathematically defined as Eq. (10):

$$H\left\{\sqrt{\frac{2}{M}} \sum_{m=0}^{M-1} \log(E_i[m]) \cos(\frac{n\pi(m-0.5)}{M})\right\} = \frac{1}{n\pi} * \sqrt{\frac{2}{M}} \sum_{m=0}^{M-1} \log(E_i[m]) \cos(\frac{n\pi(m-0.5)}{M}) \tag{10}$$

where $*$ denotes convolution. The analytic signal $z_i[n]$ can be found by Eq. (11):

$$z_i[n] = \sqrt{\frac{2}{M}} \sum_{m=0}^{M-1} \log(E_i[m]) \cos(\frac{n\pi(m-0.5)}{M}) + jH\left\{\sqrt{\frac{2}{M}} \sum_{m=0}^{M-1} \log(E_i[m]) \cos(\frac{n\pi(m-0.5)}{M})\right\} \tag{11}$$

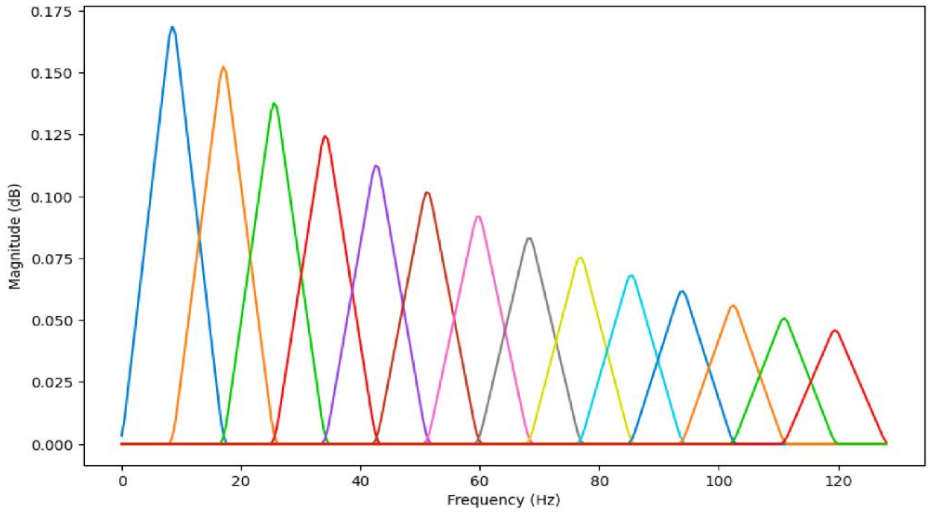

Fig. 3. Configuration of the Mel filter bank applied to the power spectrum of EEG frames, emphasizing perceptually relevant frequency bands.

where j is the imaginary unit. The instantaneous amplitude $a_i[n]$ of the analytic signal $z_i[n]$ is derived as Eq. (12):

$$a_i[n]=\left|\begin{array}{l}\sqrt{\frac{2}{M}}\sum_{m=0}^{M-1}\log(E_i[m])\cos(\frac{n\pi(m-0.5)}{M})+\\ jH\left\{\sqrt{\frac{2}{M}}\sum_{m=0}^{M-1}\log(E_i[m])\cos(\frac{n\pi(m-0.5)}{M})\right\}\end{array}\right| \quad (12)$$

The resulting amplitude envelope $a_i[n]$ are the final feature vectors used in the subsequent classification stage. These features, designed to encapsulate fine-grained spectral and temporal patterns linked to Alzheimer's pathology, are passed to various machine learning classifiers for evaluation, as thoroughly described in Section 0.

3- Experiments

3- 1- Experimental setup

The proposed model was implemented using Google Colab, a cloud-based Jupyter notebook. Tensor Processing Units (TPUs) are utilized as the runtime type. Using TPUs can significantly speed up machine learning tasks due to their ability to perform a large number of calculations simultaneously. This allowed us to train models more quickly and efficiently. The Python language is used to implement this model.

3- 2- Evaluation parameters and K-fold validation

In the field of signal processing, performance evaluation parameters are crucial for measuring the effectiveness of algorithms and models [35]. The performance of different classifiers is measured here using a range of parameters, including accuracy, specificity, precision, recall, F1-score, and geometric mean (*GM*). These parameters provide quantitative measures of how well the classifiers perform. The formulas are provided below as Eqs. (13–18):

$$Accuracy=\frac{TP+TN}{TP+TN+FP+FN} \quad (13)$$

$$Specificity=\frac{TN}{TN+FP} \quad (14)$$

$$Precision=\frac{TP}{TP+FP} \quad (15)$$

$$Recall=\frac{TP}{TP+FN} \quad (16)$$

$$F1\text{-}score=2\times\frac{Precision\times Recall}{Precision+Recall} \quad (17)$$

where TN = True Negatives, TP = True Positives, FP = False Positives, FN = False Negatives.

$$Geometric\ Mean=\sqrt[n]{x_1\cdot x_2\cdot\ \ldots\cdot x_n} \quad (18)$$

where $x_1\cdot x_2\cdot\ \ldots\cdot x_n$ are the n numbers in the dataset.

To ensure rigorous evaluation, we employed a subject-independent cross-validation strategy. Specifically, an 80/20 train–test split was applied at the subject level, where 80%

Table 3. Classification accuracy across different numbers of Mel filters, with 14 filters yielding the highest performance.

M	11	12	13	14	15	16
Accuracy	99%	99.10%	99.18%	99.24%	99.17%	99.12%

of epochs were used for training and the remaining 20% for testing. In addition, a 5-fold stratified cross-validation procedure was implemented to preserve class balance across folds. Importantly, all epochs from each subject were assigned to the same fold to avoid any leakage of subject-specific information between training and validation sets. All epochs from a given subject were kept within the same fold to completely avoid data leakage and ensure subject-level independence between training and validation sets. To further improve robustness and reduce variance caused by stochastic training effects, the entire 5-fold procedure was repeated three times using different random seeds. The final reported performance metrics represent the average across all folds and repetitions, thereby providing a more conservative and reliable estimate of classification accuracy. This design minimizes the risk of overfitting and ensures that the reported results are both stable and reproducible. Across three repetitions of 5-fold CV, each of the 9,849 epochs appears once per repetition, yielding 29,547 held-out test predictions in total. These predictions were used for computing confidence intervals and hypothesis tests. For interval estimation, we used Wilson score confidence intervals, and for hypothesis testing, we applied standard two-proportion z-tests.

3- 3- Experimental Results

To assess the proposed method's effectiveness, we conducted extensive experiments using an open-access Alzheimer's disease EEG dataset, as described in Section 2.1 [36]. This dataset contains the following frequency sub-bands: δ (0–4 Hz), θ (4–8 Hz), α (8–12 Hz), β1 (12–16 Hz), β2 (16–32 Hz), and γ (32–48 Hz). We split the dataset into 80% for training and 20% for testing. Initially, the dimension of features is 663 × 18816, which is reduced to 663 × 600 using PCA.

The selection of the optimal number of Mel filters (*M*) has significant importance in this study. Specifically, a total of 14 filters were examined, and their effect on the accuracy of the test set was analyzed, as shown in Table 3. This analysis aimed to determine the ideal number of filters for maximizing accuracy.

To identify the optimal number of Mel filters, we performed a grid search over $M \in \{11, 12, 13, 14, 15, 16\}$, recording the classification accuracy for each configuration (Table 3). As shown in Fig. 4, The classification error was minimized when using 14 filters, achieving an error rate of 0.76% (99.24% accuracy). The boundary values exhibited slightly lower performance, with accuracies of 99.10% and 99.12% for 12 and 16 filters, respectively. These results confirm that M = 14 provides the most effective filter configuration for our framework. In addition, PCA was employed to retain the top 600 components, accounting for 97.8% of the total variance. Importantly, PCA was applied before the Hilbert Transform to both reduce computational complexity and suppress noise. A comparative experiment applying PCA after the Hilbert Transform led to a minor performance drop (−0.06%), further supporting the adopted configuration.

Fig. 5 to 7 present group-averaged results across all EEG channels, reflecting aggregated patterns between AD and HC groups rather than single-subject examples. The observed qualitative contrasts are further supported by the quantitative analyses reported in the following sections. Fig. 5 presents the extracted HMFCC features for AD and HC signals, providing a detailed representation of the temporal and spectral properties. The AD features exhibit abrupt transitions and heightened variability in amplitude across consecutive frames, particularly noticeable in regions of increased spectral energy. These irregularities reflect impaired auditory feature representation and disrupted cognitive processing associated with AD. Conversely, the HC features maintain smoother transitions and consistent patterns over frames, indicative of well-regulated neural activity and stable auditory processing. The more structured and homogenous nature of HC features contrasts sharply with the fragmented and irregular patterns observed in AD, underscoring the potential of HMFS features as robust biomarkers for distinguishing between the two groups.

The spectrogram representations of AD and HC signals capture their frequency distributions; however, as depicted in Fig. 6**.** These variations are subtle and lack clear, distinguishable patterns. Both spectrograms share overlapping regions with comparable color gradients, resulting in significant challenges when attempting to differentiate between HC and AD signals based solely on their original representations. This overlap and the absence of distinct, well-defined boundaries or unique features indicate that the raw spectrograms do not provide sufficient discriminatory power for accurate classification. These observations highlight the inherent complexity of distinguishing HC from AD signals and emphasize the necessity of advanced processing or feature extraction techniques to enhance diagnostic performance.

In contrast, the spectrogram of HMFS features shown in Fig. 7 provides a much clearer distinction between the HC and AD groups. Notably, the spectrogram for HC (Fig. 7**.** a) exhibits a relatively consistent amplitude envelope, with

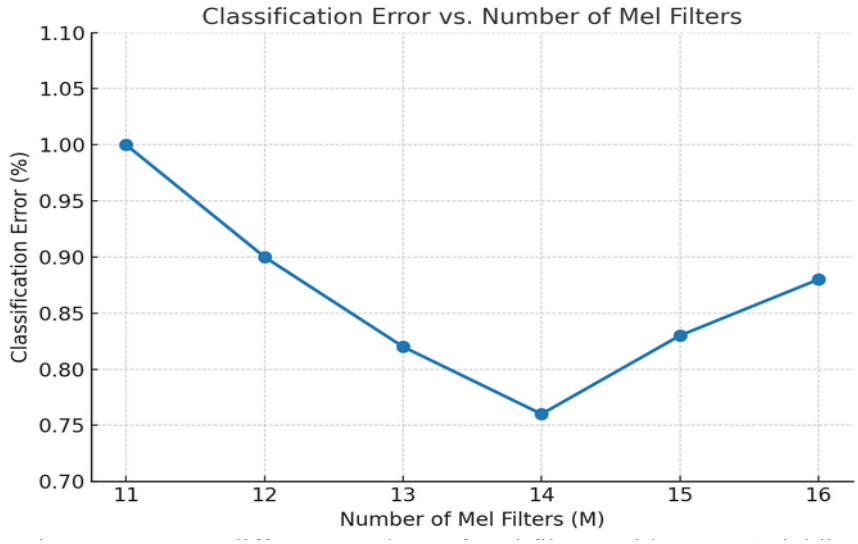

Fig. 4. Classification error across different numbers of Mel filters, with M = 14 yielding the minimum error (0.76%)

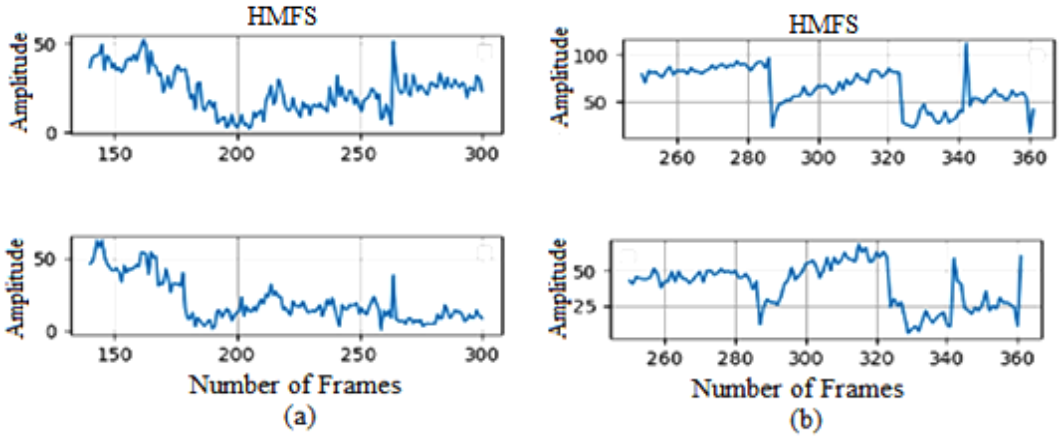

Fig. 5. Group-averaged HMFS features extracted from (a) HC and (b) AD signals, illustrating structured patterns in HC and disrupted transitions in AD.

intensity values predominantly ranging between 0.5 and 1.5 across most time frames (e.g., 100–200). In contrast, the AD spectrogram (Fig. 7**.** b) reveals pronounced irregularities, with distinct intensity shifts visible in specific regions, such as higher amplitude peaks around time frames 50–100 and a noticeable decrease in intensity between 200–250. These variations, particularly the concentrated high-intensity regions in the AD spectrogram, highlight critical differences between the two groups. Such well-defined patterns and amplitude shift significantly enhance the separability of the two classes, demonstrating the robustness of HMFS features in distinguishing AD from HC. Therefore, leveraging HMFS features provides a substantial improvement over raw signal representation for diagnostic applications.

3- 4- Classifier Selection

We evaluated the effectiveness of several classifiers, including K-Nearest Neighbors (KNN), Support Vector Machine (SVM), Decision Trees (DT), AdaBoost, Gradient Boosting, Random Forest (RF), Naive Bayes (NB), Linear Discriminant Analysis (LDA), and Cubic, using the selected features. To ensure the best classification accuracy, we

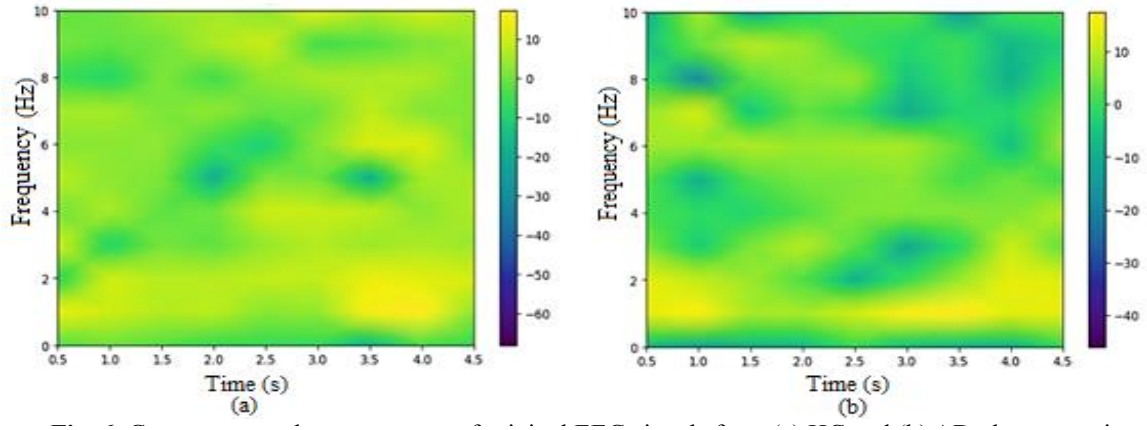

Fig. 6. Group-averaged spectrograms of original EEG signals from (a) HC and (b) AD, demonstrating overlapping frequency distributions with limited separability.

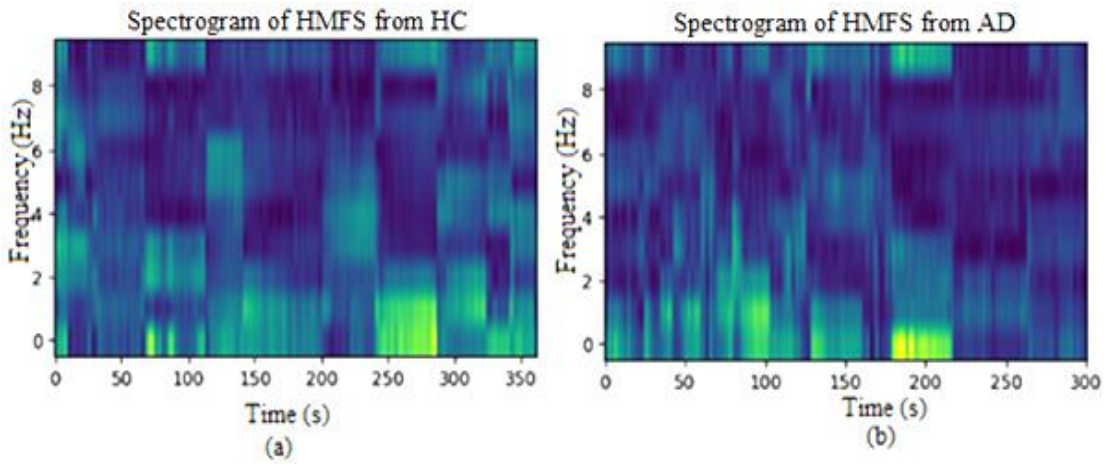

Fig. 7. Group-averaged spectrograms of HMFS features from (a) HC and (b) AD signals, indicating clearer temporal-spectral contrasts and enhanced separability between the two groups.

optimized the hyperparameters for each classifier using grid search, a systematic approach to finding the best settings.

As shown in Table 4, KNN achieved the highest accuracy at 99.24% and a perfect recall of 100%, highlighting its strong performance. The KNN model used three neighbors and the Euclidean distance to measure similarity. Other classifiers like Gradient Boosting and Cubic also performed well, with accuracy scores of 98.47% and 96.98%, respectively. However, Naive Bayes had the lowest accuracy at 69.92%.

These results suggest that KNN and a few other models are particularly effective for detecting Alzheimer's disease with the features we used. Fig. 8 presents the classification performance with error bars, which indicate variability across cross-validation folds. This suggests that KNN is particularly effective with the extracted HMFS features for distinguishing AD from HC.

To quantify statistical significance, we computed Wilson 95% confidence intervals. The proposed method achieved 99.24% accuracy (95% CI: [99.05%, 99.39%]), 100% recall for AD ([99.93%, 100%]), and 98.39% specificity for HC ([97.95%, 98.72%]). Using the full 29,547 test predictions across repeated CV, the CI narrows to [99.13%, 99.33%]. Compared to the strongest prior on the same dataset (Puri et al. [5], 98.6%), a one-sample z-test confirmed significantly higher accuracy ($z = 5.41$, $p \approx 6.4\times10^{-8}$). A two-proportion test further indicated that AD recall is significantly higher than HC specificity ($z \approx 9.59$, $p < 10^{-21}$).

To assess the performance of the proposed HMFS, we conducted further analysis by plotting the receiver operating characteristic (ROC) curve, as depicted in Fig. 9. The area under the ROC curve served as a reliable index for evaluating the effectiveness of the classifier. Notably, the

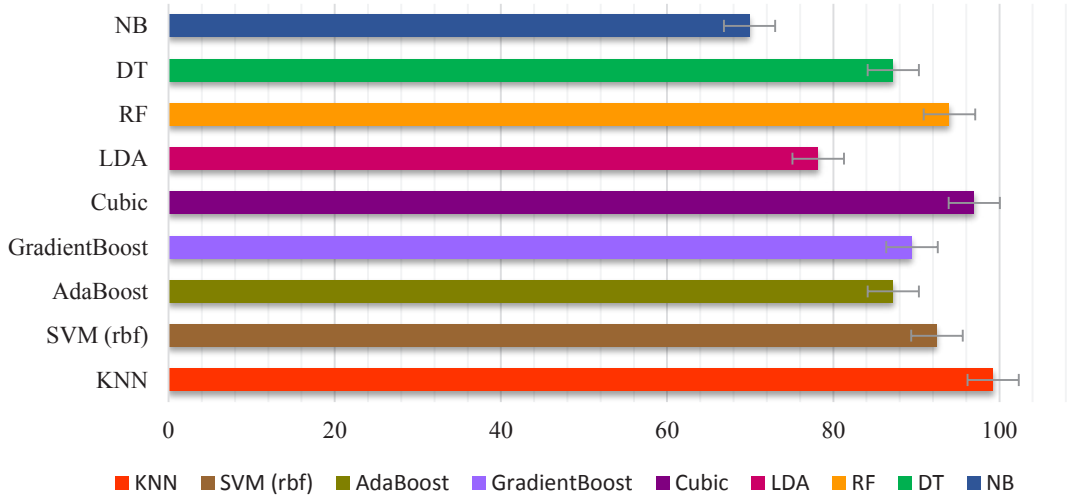

Fig. 8. Comparative performance of classifiers using HMFS features. Error bars indicate variability across cross-validation folds, with KNN achieving the highest classification accuracy.

Table 4. Performance metrics of classifiers using HMFS features, highlighting KNN as the top-performing model.

Classifier	Accuracy	Recall	precision	specificity	F1-score	GM
KNN	99.24%	100%	98.61%	98.39%	99.30%	99.31%
SVM (rbf)	92.48%	94.37%	91.78%	90.32%	93.05%	93.06%
AdaBoost	87.22%	87.33%	88.57%	87.09%	87.94%	87.94%
Gradientboost	89.47%	87.32%	92.53%	91.93%	89.85%	89.89%
Cubic	96.98%	97.37%	97.37%	96.55%	97.37%	97.37%
RF	93.98%	90.14%	98.46%	98.39%	94.11%	94.21%
DT	87.22%	87.32%	88.57%	87.09%	87.94%	87.94%
NB	69.92%	74.65%	70.67%	64.52%	72.60%	72.63%
LDA	78.19%	87.32%	75.60%	67.74%	81.04%	81.26%

KNN algorithm demonstrated the highest area under the ROC curve, indicating superior performance in comparison to other classifiers.

4- Discussion

AD, as the leading cause of dementia, poses a growing public health concern due to its progressive nature and the difficulty of early-stage detection. EEG has emerged as a promising modality for detecting functional brain changes associated with AD, offering noninvasive access to neural dynamics. In this study, a novel feature extraction pipeline based on the HMFS was proposed to enhance the diagnostic accuracy of EEG-based AD classification. The method combines the perceptually motivated Mel filter bank analysis with statistical decorrelation via Discrete DCT, dimensionality reduction using PCA, and temporal envelope tracking through the HT. This combination allows for the extraction of rich and discriminative representations that are sensitive to subtle AD-induced changes in EEG signals.

To offer a comprehensive comparative analysis, the methods detailed in Table 5 elucidate the progression of techniques for AD diagnosis using EEG signals. Early investigations, such as those by Abasolo et al. [37], relied on Approximate Entropy (AEEn), which yielded modest diagnostic metrics with recall and specificity rates of 75% and 80%, respectively. Subsequent refinements, such as the integration of AEEn with Sample Entropy (SHEn) [38], achieved incremental improvements, attaining an accuracy

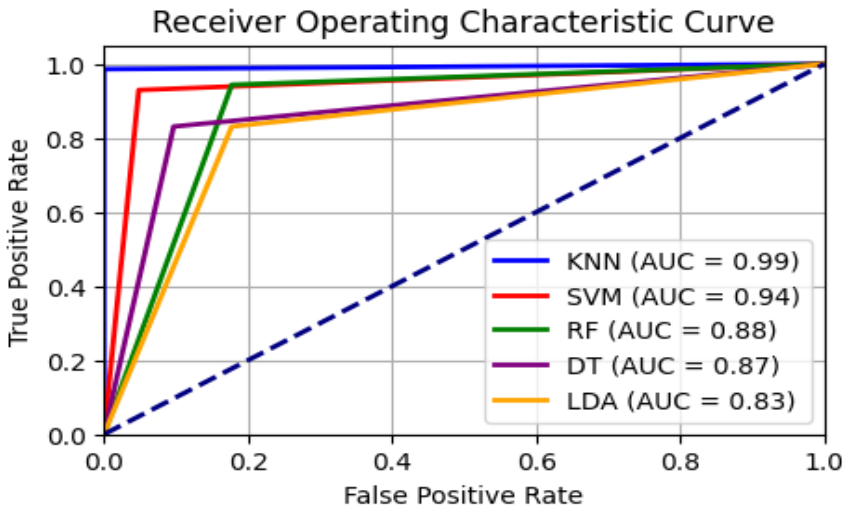

Fig. 9. ROC curves of selected classifiers, presenting superior accuracy (AUC) for KNN in distinguishing AD from healthy subjects.

of 77.27% and a recall of 90.91%, albeit at the expense of specificity, which dropped to 63.64%. Other approaches, exemplified by the combination of AEEn and Average Mutual Information (AMI) in [39], achieved flawless specificity (100%) but exhibited suboptimal recall (81.82%), underscoring the ongoing challenge of achieving balanced diagnostic performance.

Similarly, methodologies proposed by Simons et al. [40, 41], leveraging Quantitative Symbolic Entropy (QSE) and Feature Entropy (FEN), achieved accuracies of 77.27% and 86.36%, respectively, yet demonstrated a need for more harmonized sensitivity and specificity. The evolution of EEG-based diagnostic techniques has witnessed a shift toward more sophisticated methodologies and classifiers. Notable among these is the work of Durongbhan et al. [26], who employed a combination of Fast Fourier Transform (FFT) and Continuous Wavelet Transform (CWT) with k-Nearest Neighbors (KNN), achieving an exceptional accuracy of 99%. However, the absence of detailed recall and specificity metrics limits a comprehensive evaluation of its diagnostic robustness.

The contributions of Puri et al. represent significant advancements in this domain. Their approach integrates Empirical Mode Decomposition (EMD) and Hjorth parameters with Least Squares Support Vector Machines (LSSVM) [12] demonstrated a notable accuracy of 92.9%, coupled with recall and specificity rates of 94.34% and 94.32%, respectively. Another of their methods, employing Wavelet Packet Analysis (WPA) with Support Vector Machines (SVM) [43], reported an impressive accuracy of 97.5%, reflecting a robust diagnostic framework.

Subsequent innovations by Puri et al. incorporated sophisticated feature extraction techniques such as Spectral Entropy (SpecEn) with K-Means Clustering (KMC) [44] and Tunable Q-Factor Wavelet Transform (TQWT) with Extreme Boosting Trees (EBT) [45]. These methodologies achieved accuracies of 95.6% and 96.2%, respectively, with well-balanced recall and specificity metrics, reflecting significant strides in precision. The highest-performing approach among prior works, however, is attributed to their LCOWFBs-v technique combined with SVM [5], which achieved unparalleled accuracy of 98.6%, alongside recall and specificity rates of 99.8% and 97.34%, respectively. These advancements collectively underscore the trajectory of EEG-based diagnostic methodologies toward higher precision, improved balance across performance metrics, and enhanced reliability in early-stage AD detection. Recent work, such as Adazd-Net [46], reported 99.85% accuracy on the same dataset using an adaptive wavelet transform (AFAWT) with explainable ML. In comparison, the proposed HMFS framework achieves 99.24% accuracy with a far simpler pipeline, fewer hyperparameters, and intrinsic time–frequency interpretability, while also providing more stable estimates through repeated 5-fold validation. While slightly lower in accuracy (99.24%), HMFS emphasizes simplicity, stability, and interpretability, making it a practical and reproducible alternative to more complex adaptive or deep learning approaches. It should also be noted that deep learning approaches such as CNNs, RNNs, and hybrid models represent strong competitors, especially when trained with larger datasets or via transfer learning. In this study, we deliberately focused on a compact, interpretable pipeline to mitigate overfitting on small data.

The proposed method surpasses all previous approaches in terms of accuracy and recall, achieving an outstanding accuracy of 99.24%, perfect recall (100%), specificity of 98.39%, precision of 98.61%, and a GM of 99.31%. Compared to the highest-performing prior work

Table 5. Comparison of the proposed HMFS method with previous approaches on the same dataset.

Studies	Methods	Classifiers	Accuracy	Recall	Specificity
Abasolo et al. (2005) [37]	ApEN	-	-	75%	80%
Abasolo et al. (2006) [38]	SpecEN + SHEN	-	77.27%	90.91%	63.64%
Escudero et al. (2006) [42]	MSE	-	90.91%	90.91%	90.91%
Abasolo et al. (2008) [39]	ApEN + AMI	-	90.91%	81.82%	100%
Simons et al. (2015) [40]	QSE	-	77.27%	-	-
Simons et al. (2018) [41]	FEN	-	86.36%	81.82%	90.91%
Durongbhan et al. (2019) [26]	FFT + CWT	KNN	99%	-	-
Puri et al. (2022) [12]	EMD + Hjorth Parameter	LSSVM	92.9%	94.34%	94.32%
Puri et al. (2022) [43]	WPA	SVM	97.5%	97.45%	97.08%
Puri et al. (2022) [44]	SpecEn +KMC	SVM	95.6%	-	95.2%
Puri et al. (2022) [45]	TQWT	EBT	96.2%	97.5%	90.49%
Puri et al. (2023) [5]	LCOWFBs-v	SVM	98.6%	99.8%	97.34%
Khare et al. (2023) [46]	AFAWT	XBM	99.85%	99.75%	100%
Proposed method	**HMFS**	**KNN**	**99.24%**	**100%**	**98.39%**

(LCOWFBs-v) by Puri et al. [5], The proposed method not only achieves higher recall but also offers superior F1-score and GM, indicating a better balance between sensitivity and specificity. This comprehensive comparison demonstrates the effectiveness and robustness of the proposed method, positioning it as a superior diagnostic tool for AD detection.

Another important aspect is finding the optimal number of Mel filters for classification accuracy. After extensive testing, we found that 14 Mel filters produced the best results, showing the value of tuning signal processing parameters to help the model distinguish between AD patients and healthy controls. Using PCA improved both efficiency and effectiveness by keeping essential features while reducing noise and redundant data. This ultimately enhanced the performance of the analysis. The classification phase of the study showed that the KNN algorithm achieved the highest accuracy at an impressive 99.24%. This strong performance was further supported by the highest AUC, confirming KNN's effectiveness in distinguishing between AD and NC subjects. Compared to other classifiers and existing methods, the HMFS method showed significant improvements in both accuracy and reliability.

To further validate the robustness of the proposed method, statistical analyses were conducted on the classification outcomes. The overall accuracy of 99.24% corresponds to a 95% confidence interval of [99.05%, 99.39%] at the epoch level. When aggregating predictions across repeated cross-validation (29,547 test instances), the interval narrows to [99.13%, 99.33%], reflecting the stability of performance across folds and repetitions. Class-wise analysis revealed perfect recall for AD (100%, CI [99.93%, 100%]) and high specificity for HC (98.39%, CI [97.95%, 98.72%]). A two-proportion significance test confirmed that recall for AD was statistically higher than specificity for HC, suggesting that the model identifies AD more readily while still maintaining excellent specificity. These findings highlight the consistency and discriminative power of the HMFS features and demonstrate that the performance gains are not attributable to random variation.

5- Conclusion

This study introduced a novel and effective feature extraction framework for EEG-based diagnosis of Alzheimer's disease, leveraging a combination of Mel Cepstral analysis and the HT. The method first captured perceptually meaningful frequency-domain representations using Mel filter banks, followed by decorrelation via DCT and dimensionality reduction through PCA. To further enhance temporal resolution, the Hilbert Transform was applied to extract the instantaneous amplitude of the signal, resulting in highly informative temporal envelopes that reflect pathological EEG dynamics associated with AD. The proposed approach was comprehensively evaluated using multiple classifiers, including KNN, SVM, and RF. Among them, KNN achieved the highest performance, reaching an accuracy of 99.24% in distinguishing between Alzheimer's patients and healthy controls. The method also demonstrated excellent diagnostic reliability across other metrics, achieving 100% recall, 98.61% precision, 98.39% specificity, an F1-score of 99.30%, and a geometric mean of 99.31%. By offering a strong balance between interpretability, computational efficiency, and diagnostic precision, the proposed HMFS-based framework provides a promising foundation for real-time, EEG-based screening and monitoring of AD. Future work will aim to validate the approach on larger and more diverse datasets and explore its applicability in early-stage and multi-class neurodegenerative classification tasks. Future work will extend the HMFS framework to multiclass dementia classification (e.g., AD vs. FTD vs. HC), incorporate multimodal biomarkers, evaluate the method on larger multi-center datasets, and explore hybrid models that integrate HMFS with adaptive transforms and deep neural architectures. In addition, we plan to evaluate the HMFS framework on larger multi-center EEG datasets as they become available, to further validate generalizability across diverse populations.

References

[1] Alzheimer Association, Stages of Alzheimer's disease, in 2023.

[2] World Health Organization, Dementia, in 2023.

[3] Breijyeh, Z., Karaman, R., Comprehensive review on Alzheimer's disease: causes and treatment, Molecules, 25(24) (2020).

[4] Ding, Y., Chu, Y., Liu, M., Ling, Z., Wang, S., Li, X., and Li, Y, Fully automated discrimination of Alzheimer's disease using resting-state electroencephalography signals, Quantitative imaging in medicine and surgery, 12(2) (2022).

[5] Puri, D.V., Nalbalwar, S.L., Nandgaonkar, A.B., Gawande, J.P., and Wagh, A., Automatic detection of Alzheimer's disease from EEG signals using low-complexity orthogonal wavelet filter banks, Biomedical Signal Processing and Control, 81 (2023) 104439.

[6] Calub, G.I.A., Elefante, E.N., Galisanao, J.C.A., Iguid, S.L.B.G., Salise, J.C., Prado, S.V., EEG-based classification of stages of Alzheimer's disease (AD) and mild cognitive impairment (MCI), in: 5th International Conference on Bio-engineering for Smart Technologies, IEEE, 2023, pp. 1–6.

[7] Modir, A., Shamekhi, S., and Ghaderyan, P., A systematic review and methodological analysis of EEG-based biomarkers of Alzheimer's disease. , Measurement, 220 (2023) 113274.

[8] Song, Z., Deng, B., Wang, J. and Yi, G., An EEG-based systematic explainable detection framework for probing and localizing abnormal patterns in Alzheimer's disease, Journal of Neural Engineering, 19(3) (2022) 036007.

[9] Cura, O.K., Akan, A., Yilmaz, G.C., Ture, H.S., Detection of Alzheimer's dementia by using signal decomposition and machine learning methods, International Journal of Neural Systems, 32(9) (2022) 2250042.

[10] Desai, S., Bharati, A., Early detection of Alzheimer's using EEG, International Journal of Computer Science and Mobile Computing, 12(3) (2023) 34–39.

[11] Sadegh-Zadeh, S.A., Fakhri, E., Bahrami, M., Bagheri, E., Khamsehashari, R., Noroozian, M., and Hajiyavand, A.M., An approach toward artificial intelligence Alzheimer's disease diagnosis using brain signals, Diagnostics, 13(3) (2023) 477.

[12] Puri, D., Nalbalwar, S., Nandgaonkar, A., Kachare, P., Rajput, J., and Wagh, A, Alzheimer's disease detection using empirical mode decomposition and Hjorth parameters of EEG signal, in: International Conference on Decision Aid Sciences and Applications (DASA), IEEE, 2022, pp. 9765111.

[13] Vicchietti, M.L., Ramos, F.M., Betting, L.E., and Campanharo, A.S., Computational methods of EEG signals analysis for Alzheimer's disease classification, Scientific Reports, 13(1) (2023) 8184.

[14] Jiao, B., Li, R., Zhou, H., Qing, K., Liu, H., Pan, H., Lei, Y., Fu, W., Wang, X., Xiao, X. and Liu, X.,, Neural biomarker diagnosis and prediction to mild cognitive impairment and Alzheimer's disease using EEG technology, Alzheimer's research & therapy, 15(1) (2023) 32.

[15] AlSharabi, K., Bin Salamah, Y., Abdurraqeeb, A.M., Aljalal, M., Alturki, F.A., EEG signal processing for Alzheimer's disorders using discrete wavelet transform and machine learning approaches, IEEE Access, 10 (2022) 17.

[16] Xia, W., Zhang, R., Zhang, X., and Usman, M., A novel method for diagnosing Alzheimer's disease using deep pyramid CNN based on EEG signals, Heliyon, 9(4) (2023) 14858.

[17] Houmani, N., Vialatte, F., Gallego-Jutglà, E., Dreyfus, G., Nguyen-Michel, V.H., Mariani, J. and Kinugawa, K., Diagnosis of Alzheimer's disease with electroencephalography in a differential framework, PloS one, 13(3) (2018) e0193607.

[18] Chen, Y., Wang, H., Zhang, D., Zhang, L., and Tao, L., Multi-feature fusion learning for Alzheimer's disease prediction using EEG signals in resting state, Frontiers in neuroscience, 17 (2023) 1272834.

[19] Alessandrini, M., Biagetti, G., Crippa, P., Falaschetti, L., Luzzi, S. and Turchetti, C., EEG-based Alzheimer's disease recognition using robust-PCA and LSTM recurrent neural network, Sensors, 22(10) (2022) 3696.

[20] Sharma, G., Parashar, A. and Joshi, A.M., DepHNN: A novel hybrid neural network for electroencephalogram (EEG)-based screening of depression, Biomedical signal processing and control, 66 (2021) 102393.

[21] Sekhar, J.C., Rajyalakshmi, C., Nagaraj, S., Sankar, S., Saturi, R., and Harshavardhan, A., Deep generative adversarial networks with marine predators algorithm for classification of Alzheimer's disease using electroencephalogram, Journal of King Saud University-Computer and Information Sciences, 35(10) (2023) 101848.

[22] Cao, J., Yang, L., Sarrigiannis, P.G., Blackburn, D., and Zhao, Y., Dementia classification using a graph neural network on imaging of effective brain connectivity, Computers in Biology and Medicine, 168 (2024) 107701.

[23] Al-Nuaimi, A.H.H., Jammeh, E., Sun, L. and Ifeachor, E., Complexity measures for quantifying changes in electroencephalogram in Alzheimer's disease, Complexity, 1 (2018) 8915079.

[24] Pirrone, D., Weitschek, E., Di Paolo, P., De Salvo, S., De Cola, M.C., EEG signal processing and supervised machine learning to early diagnose Alzheimer's disease, Applied sciences, 12(11) (2022) 5413.

[25] Kulkarni N.N., Bairagi, V.K., Extracting salient features for EEG-based diagnosis of Alzheimer's disease using support vector machine classifier, IETE Journal of Research, 63(1) (2017) 12.

[26] Durongbhan, P., Zhao, Y., Chen, L., Zis, P., De Marco, M., Unwin, Z.C., Venneri, A., He, X., Li, S., Zhao, Y. and Blackburn, D.J.,, A dementia classification framework using frequency and time-frequency features based on EEG signals, IEEE Transactions on Neural Systems and Rehabilitation Engineering, 27(5) (2019) 826–835.

[27] Chen, Y.L., Wang, N.C., Ciou, J.F. and Lin, R.Q., Combined bidirectional long short-term memory with Mel-frequency cepstral coefficients using autoencoder for speaker recognition, Applied Sciences, 13(12) (2023) 7008.

[28] Abbaskhah, A., Sedighi, H., Marvi, H., Infant cry classification by MFCC feature extraction with MLP and CNN structures, Biomedical Signal Processing and Control, 86 (2023) 105261.

[29] Sai, V., Abdul Majeed, K.K.,, Advancements in speaker recognition: Exploring Mel-frequency cepstral coefficients (MFCC) for enhanced performance in speaker recognition, International Journal for Research in Applied Science & Engineering Technology (IJRASET), 11 (2023) 88–98.

[30] Gao, D., Tang, X., Wan, M., Huang, G., Zhang, Y., EEG driving fatigue detection based on log-Mel spectrogram and convolutional recurrent neural networks, Frontiers in Neuroscience, 17 (2023) 1136609.

[31] Hosseinzadeh, M., Haider, A., Malik, M.H., Adeli, M., Mzoughi, O., Gemeay, E., Mohammadi, M., Alinejad-Rokny, H., Khoshvaght, P., Porntaveetus, T., and Rahmani, A.M., Enhanced heart sound classification using Mel frequency cepstral coefficients and comparative analysis of single vs. ensemble classifier strategies, PloS one, 19(12) (2024) e0316645.

[32] AD-NC EEG database, in, 2025.

[33] Safi, M.S., Safi, S.M.M., Early detection of Alzheimer's disease from EEG signals using Hjorth parameters, Biomedical Signal Processing and Control, 65 (2021) 102338.

[34] Oltu, B., Akşahin, M.F. and Kibaroğlu, S.,, A novel electroencephalography-based approach for Alzheimer's disease and mild cognitive impairment detection, Biomedical Signal Processing and Control, 63 (2021) 102223.

[35] Fiscon, G., Weitschek, E., De Cola, M.C., Felici, G. and Bertolazzi, P., An integrated approach based on EEG signals processing combined with supervised methods to classify Alzheimer's disease patients, in: IEEE International Conference on Bioinformatics and Biomedicine (BIBM) 2018, pp. 2750–2752.

[36] Smith, K., Abásolo, D. and Escudero, J., Accounting for the complex hierarchical topology of EEG phase-based functional connectivity in network binarization, PLoS One, 12(10) (2017) e0186164.

[37] Abásolo, D., Hornero, R., Espino, P., Poza, J., Sánchez, C.I., and de la Rosa, R, Analysis of regularity in the EEG background activity of Alzheimer's disease patients with approximate entropy, Clinical neurophysiology, 116(8) (2005) 1826–1834.

[38] Abásolo, D., Hornero, R., Espino, P., Alvarez, D. and Poza, J., Entropy analysis of the EEG background activity in Alzheimer's disease patients, Physiological measurement, 27(3) (2006) 241.

[39] Abasolo, D., Escudero, J., Hornero, R., Gómez, C. and Espino, P., Approximate entropy and auto mutual information analysis of the electroencephalogram in Alzheimer's disease patients, Medical & biological engineering & computing, 46(10) (2008) 1019–1028.

[40] Simons, S., Abasolo, D. and Escudero, J., Classification of Alzheimer's disease from quadratic sample entropy of electroencephalogram, Healthcare technology letters, 2(3) (2015) 70–73.

[41] Simons, S., Espino, P., and Abásolo, D., Fuzzy entropy analysis of the electroencephalogram in patients with Alzheimer's disease: Is the method superior to sample entropy?, Entropy, 20(1) (2018) 21.

[42] Escudero, J., Abásolo, D., Hornero, R., Espino, P., and López, M., Analysis of electroencephalograms in Alzheimer's disease patients with multiscale entropy, Physiological measurement, 27(11) (2006) 1091.

[43] Puri, D., Nalbalwar, S., Nandgaonkar, A. and Wagh, A., Alzheimer's disease detection with optimal EEG channel selection using wavelet transform, in: International Conference on Decision Aid Sciences and Applications (DASA) IEEE, 2022, pp. 443–448

[44] Puri, D., Nalbalwar, S., Nandgaonkar, A. and Wagh, A., EEG-based diagnosis of Alzheimer's disease using Kolmogorov complexity, in: Applied Information Processing Systems: Proceedings of ICCET, Springer Singapore, Singapore, 2021, pp. 157–165.

[45] Puri, D., Nalbalwar, S., Nandgaonkar, A., and Wagh, A., Alzheimer's disease detection from optimal electroencephalogram channels and tunable Q-wavelet transform, Indo. J. Elec. Engg. Comp. Sci, 25(3) (2022) 1420–1428.

[46] Khare, S. K., and Acharya, U. R., Adazd-Net: Automated adaptive and explainable Alzheimer's disease detection system using EEG signals. Knowledge-Based Systems, Knowledge-Based Systems, 278 (2023) 110858.

HOW TO CITE THIS ARTICLE
M. Bahmani, H. Marvi, H. Khosravi, V. Abolghasemi, Hilbert-Mel Frequency Spectrum Features for Efficient EEG-Based Alzheimer's Detection, AUT J. Elec. Eng., 58(1) (2026) 59-74.

DOI: 10.22060/eej.2025.24329.5685